arXiv:1209.5253v2 [cond-mat.supr-con] 10 Oct 2012

Electron-phonon superconductivity in $A\mathrm{Pt}_3\mathrm{P}$ compounds: from weak to strong coupling

Alaska Subedi, Luciano Ortenzi, and Lilia Boeri
Max Planck Institute for Solid State Research, Heisenbergstr. 1, D-70569 Stuttgart, Germany

We study the newly-discovered Pt phosphides $A\mathrm{Pt}_3\mathrm{P}$ (A=Sr, Ca, La) [*T. Takayama, et al., Phys. Rev. Lett.* **108**, *237001*] using first-principles calculations and Migdal-Eliashberg theory. We exclude the charge-density wave scenario proposed by previous first-principles calculations. Instead, we find that all three compounds are well described by conventional s-wave superconductivity. The pairing increases from La to Ca and Sr due to changes in the electron-phonon matrix elements and low frequency phonons. Our picture is fully supported by comparison with the available experimental data. This allows us to rule out exotic and multiband contributions to the superconducting pairing.

In the last ten years, several important discoveries have sensibly advanced our understanding of superconductivity. At the same time, ideas percolating from other fields of condensed matter have brought in new twists into this old and fascinating phenomenon. For example, the recent interest in spin-orbit coupling (SOC) [1] has revived the discussion on superconductivity in non-centrosymmetric crystals (NCSC) [2, 3], boosted by the discovery of the heavy fermion $\mathrm{CePt}_3\mathrm{Si}$ (T_c=0.75 K) in 2004 [4]. In crystals without inversion symmetry, a strong antisymmetric SOC that lifts the spin degeneracy can be conducive to exotic pairing symmetry. Because of the large SOC of Pt ($Z = 78$), this makes Pt-based compounds promising candidates for exotic superconductivity, as discussed for SrPtAs [5, 6].

Recently, Takayama *et al.* discovered a new family of ternary platinum phosphide superconductors with chemical formula $A\mathrm{Pt}_3\mathrm{P}$ (A = Sr, Ca, and La) and T_c's of 8.4 K, 6.6 K and 1.5 K, respectively [7]. Besides the relatively high T_c, these compounds exhibit a very interesting crystal structure, which is a centrosymmetric variant of the $\mathrm{CePt}_3\mathrm{Si}$ one. The authors have suggested that this discovery would have a very strong impact in the field of superconductivity if one could synthesize both centrosymmetric and non-centrosymmetric variants of superconductors consisting of the electronically equivalent elements. This would in fact allow to study the effect of inversion symmetry on superconductivity in a controlled way.

The nature of the superconducting pairing in the $A\mathrm{Pt}_3\mathrm{P}$ compounds has been debated through experiments [7] and *ab initio* calculations [8, 9]. In the original discovery paper, it was proposed that, at least in $\mathrm{SrPt}_3\mathrm{P}$, the superconductivity is of strong-coupling s-wave type with clear signatures of low-lying phonons and some indications of multiband behavior. The authors of Ref. 8 have instead proposed that T_c is enhanced by the proximity to a dynamical charge-density wave (CDW) instability, and that a strong SOC could eventually lead to *exotic* superconductivity in $\mathrm{LaPt}_3\mathrm{P}$.

In this Letter, we employ first principles calculations and Migdal-Eliashberg theory to study superconductivity in the $A\mathrm{Pt}_3\mathrm{P}$ phosphides [10, 11]. We find that SOC plays a marginal role in all three compounds and show that the available experimental data are quantitatively reproduced by conventional *ep* theory [12]. This rules out exotic pairing and CDW instabilities [8]. In fact, the $A\mathrm{Pt}_3\mathrm{P}$ series is a textbook example for *ep* superconductivity: $\mathrm{LaPt}_3\mathrm{P}$, where T_c is only 1.5 K, is a typical low-T_c superconductor in which all phonon branches are moderately coupled to the electrons at E_F. Lowering the electronic filling from trivalent La to divalent Sr and Ca brings about an intense *ep* coupling that is concentrated in low-lying phonon branches with substantial Pt in-plane breathing character. In $\mathrm{SrPt}_3\mathrm{P}$, these branches are flat and have low frequencies, and this entirely explains the large value of its BCS ratios [7, 13].

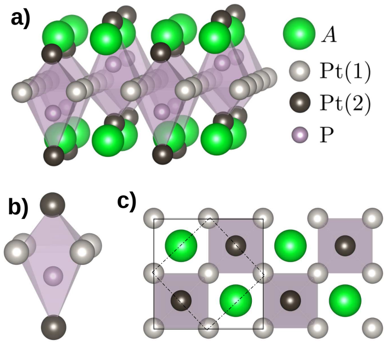

FIG. 1. (Color online) (a) Crystal structure of $A\mathrm{Pt}_3\mathrm{P}$, space group $P4/nmm$. The $\sqrt{2} \times \sqrt{2}$ in-plane arrangement of the distorted $X\mathrm{Pt}_6$ octahedra (b) distinguishes the $A\mathrm{Pt}_3\mathrm{P}$ compounds from the non-centrosymmetric $\mathrm{CePt}_3\mathrm{Si}$ superconductor (space group $P4mm$); the corresponding unit cells are shown as full and dashed lines in panel (c).

We employed the experimental crystal structure in space group $P4/nmm$ as depicted in Fig. 1(a) [14] with fully relaxed lattice parameters and internal coordinates. In these tetragonal antiperovskites $A\mathrm{Pt}_3X$, the ionic radii of Pt and X ions are similar, and the X ions off-center from the octahedral basal plane formed by the Pt(1) ions as the X ion is too big to fit into the center of the Pt(1) square. The apical Pt(2) ion that is further from the X ion also moves closer to the basal plane to ensure closer packing of the constituent ions.This distortion of the $X\text{Pt}_6$ octahedra occurs in both the phosphides (X=P) and in the non-centrosymmetric rare-earth silicides $R\text{Pt}_3\text{Si}$ (R=La,Ce) with space group $P4mm$. In the silicides, the distortions have a *polar* arrangement, *i.e.* they all point in the same direction. The corresponding unit cell that contains one formula unit (*f.u.*) is shown with dashed lines in Fig. 1(c). With full lines we show the $\sqrt{2} \times \sqrt{2}$ cell of the phosphides, where the distortions alternate in a checkerboard fashion and restore the inversion symmetry (*antipolar* structure). At zero pressure, we find a quite small (~ 10 meV) energy difference between polar and antipolar arrangements, hinting that it might be possible to tune the polar arrangement of the octahedra.

Our electronic structures are in very good agreement with previous calculations [8, 9]. A zoom-in of the bands for energies ±1 eV around the Fermi level (E_F) is shown in Fig. 2 with (red, dashed) and without (black, solid) SOC. Only in LaPt_3P does the SOC lead to a visible lifting of some band degeneracies. But even in this case, the bands remain spin degenerate, in contrast to what is claimed by Ref. 8. The densities of states (DOS) at E_F are $N(0) \sim 2.36$ st/eV f.u. in Sr, 2.37 in Ca and 1.94 in La, and the SOC changes them by less than 5 %. Since the SOC plays only a marginal role on the electronic states near E_F, we neglect it in the following.

In the A^{2+} compounds, the Fermi surface (not shown) comprises a large low dispersive sheet with prominent Pt(1) character and two more dispersive pockets with more Pt(2), P and interstitial character. Since the sheets are degenerate along certain sections and the orbital character along the sheets varies smoothly, genuine multiband superconductivity, as proposed by Ref. 7, is highly unlikely, but the unequal distribution of the orbital characters on the FS sheets could lead to anisotropic superconductivity. LaPt_3P, with one more electron per *f.u.* has its Fermi level shifted up by ∼0.5 eV, and the band with low dispersion along $M - \Gamma$ is completely full. The Fermi surface is composed of highly dispersive sheets, with strongly mixed orbital contributions of Pt(2), P and Pt(1) characters.

The phonon dispersions are shown in Fig. 3. The thirty phonon branches are divided into a lower manifold of twenty-four bands extending up to 200 cm^{-1}, an intermediate group of four phonon bands at ~ 300 cm^{-1} that show mostly in-plane vibration of P, and two uppermost bands with mostly out-of-plane P character between 390 and 420 cm^{-1}. In SrPt_3P, within the manifold of the twenty-four intertwined lower bands, the bands upto 60 cm^{-1} show mainly in-plane Pt(1) vibrations. The modes between 60 and 120 cm^{-1} have mixed Sr, Pt(1), Pt(2), and P character, while Sr character dominates the modes between 120 and 170 cm^{-1}. Overall, the phonon dispersions of CaPt_3P and LaPt_3P are very similar, except for slight redistributions of the spectral weight. The phonon frequencies are slightly higher in CaPt_3P due to its smaller volume. In LaPt_3P, due to the larger mass of La, the La modes lie at lower frequencies and mix with Pt(1) and Pt(2) modes.

On the other hand, there is a substantial difference in the Eliashberg functions, plotted in the rightmost panels of Fig. 3 and defined as:

$$\alpha^2F(\omega) = \frac{1}{N(0)} \sum_{\mathbf{k},\mathbf{q},\nu,n,m} \delta(\epsilon^n_{\mathbf{k}})\delta(\epsilon^m_{\mathbf{k+q}})|g^{\nu,n,m}_{\mathbf{k},\mathbf{k+q}}|^2\delta(\omega-\omega_{\nu\mathbf{q}}), \tag{1}$$

where $\omega_{\nu\mathbf{q}}$ are phonon frequencies, $\epsilon^n_{\mathbf{k}}$ electronic energies, and $|g^{\nu,n,m}_{\mathbf{k},\mathbf{k+q}}|^2$ *ep* matrix elements. The $\alpha^2F(\omega)$ yield information not only on the intensity of the total *ep* coupling (EPC) λ, but also on the nature of the bonding and character of the superconducting state. In general, an $\alpha^2F(\omega)$ roughly proportional to the PDOS is characteristic of metals with a weak to moderate total coupling and low $T_c's \lesssim 5$ K. The best *ep* superconductors, such as MgB_2 and A15's, are instead characterized by sharp peaks in their $\alpha^2F(\omega)$, reflecting a strong coupling between specific electron and phonon states. This requires (partly) covalent bonding and obeys clear symmetry considerations. It is not uncommon that within the same family of materials the electron count changes the *ep* coupling regime from weak to strong, depending on the nature of the electronic states at E_F in Eq. 1.

Fig. 3 shows that while the coupling is uniform in LaPt_3P, in the two A^{2+} compounds it is strongly enhanced at low frequencies. Furthermore, it is almost entirely concentrated in the low-lying phonon branches with substantial Pt in-plane breathing character. These modes are very low in energy and almost dispersionless in SrPt_3P ($\omega \sim 50$ cm^{-1}) and slightly harder in Ca, where they have a sizable dispersion that extends up to ∼100 cm^{-1}. One can trace their evolution in the two compounds by following the largest $\lambda_{\mathbf{q},\nu}$ symbols that decorate the phonon dispersions, or looking at the partial Pt(1) phonon DOS plotted in the middle panel of Fig. 3.

In-plane Pt breathing modes couple more strongly to the Pt(1) in-plane electronic states, which contribute to a large part of the $A^{2+}\text{Pt}_3\text{P}$ Fermi surface, but much less to that of LaPt_3P. This causes some anisotropy in the $\mathbf{k}$ space distribution of the EPC and, as a consequence, in the $\mathbf{q}$-dependence of the $\lambda_{\mathbf{q},\nu}$.

The total EPC constant $\lambda = \sum_{\mathbf{q},\nu} \lambda_{\mathbf{q},\nu} = 2\int_0^\infty \frac{\alpha^2F(\omega)}{\omega} d\omega$ is quite low in LaPt_3P ($\lambda = 0.57$) but sizable both in CaPt_3P ($\lambda = 0.85$) and SrPt_3P ($\lambda = 1.33$). Due to the $1/\omega$ factor, the EPC is strongly enhanced in SrPt_3P with respect to CaPt_3P because a considerable part of the breathing branches is shifted to low frequencies. For some $\mathbf{q}$ points where the differences in $\omega_{\mathbf{q},br}$ are large, the partial EPC constants $\lambda_{\mathbf{q},br} = const \times I_{\mathbf{q},br}/\omega^2_{\mathbf{q},br}$ differ by as much as a factor three despite a very small difference ($\sim 10\%$) in the matrix elements (I_{br}), as shown in table I for the Γ point. The

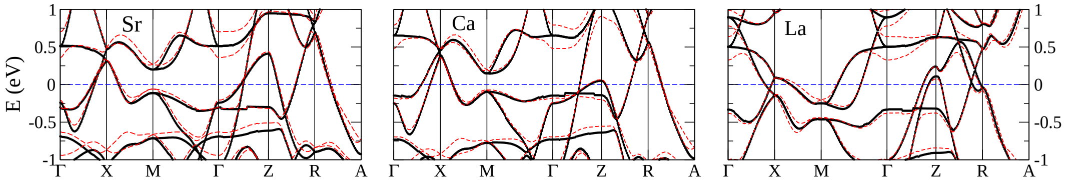

FIG. 2. (Color online) Electronic structure of $A\mathrm{Pt}_3\mathrm{P}$ with (red, dashed line) and without (black, solid line) spin orbit coupling (SOC); the zero of the energy is the Fermi level.

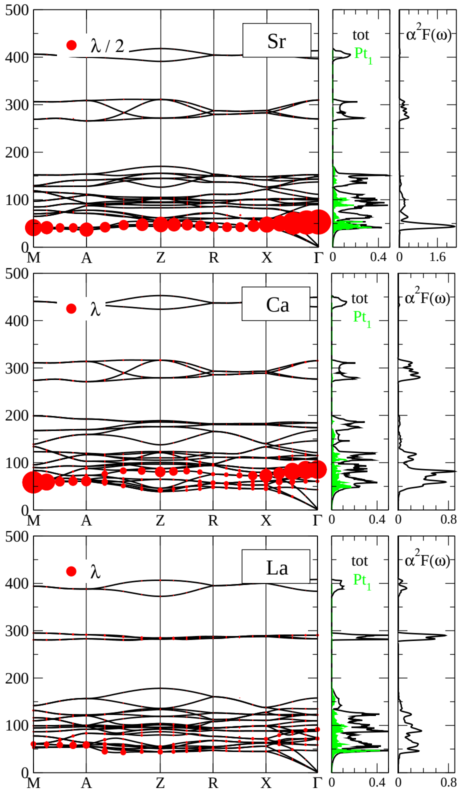

FIG. 3. (Color online) Phonon dispersions, density of states and Eliashberg function $\alpha^2F(\omega)$ of $A\mathrm{Pt}_3\mathrm{P}$. The phonon dispersions are decorated with symbols, proportional to the partial *ep* coupling $\lambda_{\mathbf{q}\nu}$; for readability, the λ's for Sr have been rescaled by a factor two. The logarithmically averaged phonon frequencies $\omega_{\ln}$, the *ep* coupling constants λ, and the corresponding critical temperatures T_c's are given in table II.

small difference in the EP matrix elements implies that the lowering of the frequencies in Sr with respect to Ca is not due to increased EP coupling. Instead, we find that this is related to the decrease of the in-plane lattice constant a. This is discussed in detail also in Ref. 8 [15].

Changing the dispersion of the breathing branch through the in-plane lattice constant also turns the regime for superconductivity from weak coupling in Ca to strong coupling in Sr, despite the very close critical temperatures. In fact, the shift of spectral weight in $\alpha^2F(\omega)$ to lower energies causes a strong enhancement in λ, but it also induces a decrease in $\omega_{\ln} = \exp\left(\frac{2}{\lambda}\int_0^\infty d\omega/\omega\alpha^2F(\omega)\ln\omega\right)$ – see Table I. These two factors compensate in the Allen-Dynes expression for T$_c$:

$$T_c = \frac{\omega_{\ln}}{1.20}\exp\left(-\frac{1.04(1+\lambda)}{\lambda-\mu^*-0.62\lambda\mu^*}\right),$$

but not in the BCS ratios ($2\Delta/T_c$, $\Delta C/T_c$, etc.), which to a very good approximation depend only on the ratio $T_c/\omega_{\ln}$, used to classify conventional superconductors [13]. $\mathrm{LaPt}_3\mathrm{P}$ and $\mathrm{CaPt}_3\mathrm{P}$, with $T_c/\omega_{\ln}$=0.013 and 0.058, respectively, are in line with typical elemental metals. $\mathrm{SrPt}_3\mathrm{P}$ ($T_c/\omega_{\ln} = 0.110$) is placed at the lower end of a broad class of low-phonon, strong-coupling superconductors together with the A15 and Chevrel compounds.

TABLE I. Some calculated results for $A\mathrm{Pt}_3\mathrm{P}$: Electronic density of states at the Fermi level $N(0)$ in states/eV/spin/unit cell; $\omega_{\ln}$ in K; Frequency ω_{br} in cm^{-1}, e-ph coupling λ_{br}, and e-ph coupling strength I_{br} in cm^{-2} for the in-plane Pt(1) breathing mode at Γ.

	$N(0)$	λ	$\omega_{\ln}$	ω_{br}	λ_{br}	I_{br}
$\mathrm{SrPt}_3\mathrm{P}$	2.36	1.33	77	53.0	1.90	5337
$\mathrm{CaPt}_3\mathrm{P}$	2.37	0.85	110	85.5	0.63	4605
$\mathrm{LaPt}_3\mathrm{P}$	1.94	0.57	118	91.5	0.14	1172

From electronic structure calculations, we have concluded that $A\mathrm{Pt}_3\mathrm{P}$ phosphides are *ep* superconductors in which the superconducting regime can be *tuned* by varying the in-plane lattice constant. The analysis of the specific heat data of Ref. 7 in terms of the single-band Migdal Eliashberg theory will now allow us to address the dynamical stability of low-lying phonons and the relevance of multiband or anisotropic superconductivity in $\mathrm{SrPt}_3\mathrm{P}$.

The inset of Fig. 4 compares calculations (solid lines) and experiments (symbols) for the total normal state specific heat. The remarkable agreement suggests that our calculated phonon spectra are very close to the actual ones, ruling out the dynamical instabilities calculated in Ref. 8. In the main panel of the figure, the superconducting state data for $\mathrm{SrPt}_3\mathrm{P}$ are shown as blue curves. The calculations reproduce almost exactly the experimental curve, indicating that the large $\frac{2\Delta}{T_c} \sim 5$ of Ref. 7 is an artefact of the simplified α model employed to fit the data, and the actual value of the gap is much lower $\frac{2\Delta}{T_c} \sim 4.06$. This sensibly reduces the room for multiband superconductivity and excludes anisotropic effects suggested from electronic structure calculations, although the anisotropy could be washed out by the impurity scattering in the real samples.

As for the low-T_c compounds, we again obtain critical temperatures in very good agreement with experiments, which is a strong indication in favor of conventional superconductivity. $CaPt_3P$ (red curves in Fig. 4) displays a mass enhancement in the normal state that is 2.5 times larger than the calculated one, which we attribute to the presence of additional superconducting phases in the sample. All other quantities are in line with our calculations. In fact, using the calculated value of $\gamma_N = 10.3$ mJ mol^{-1} K^{-2}, we obtain also a reasonable fit to the specific heat jump. For $LaPt_3P$ (green curves in Fig. 4) we obtain a fairly good agreement for the normal state quantities, while the superconducting state data are probably too noisy for a meaningful comparison.

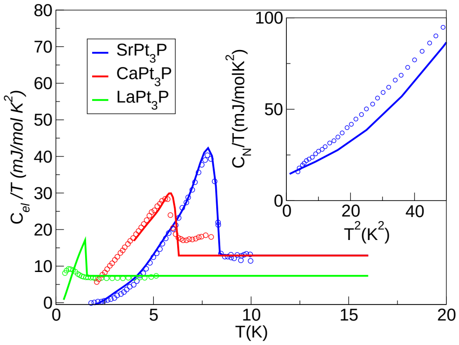

FIG. 4. (Color online) Comparison between experimental data from Ref. 7 (colored dots) and Migdal Eliashberg theory (colored lines) for the heat capacities of APt_3P (A = Sr, Ca and La). Inset: Comparison between experimental data from Ref. 7 (blue dots) and first-principles calculations (blue line) for the normal state specific heat of $SrPt_3P$.

TABLE II. Superconducting properties of APt_3P, from first-principles calculations and Migdal-Eliashberg theory; γ_N is the electronic normal-state specific heat, in mJ mol^{-1} K^{-2}, $\Delta(0)$ is the value of the superconducting gap, ΔC is the specific heat jump at T_c. Experimental data from Ref. 7 are in parentheses. The Coulomb pseudopotential μ^* was fixed to reproduce the experimental T_c.

	γ_N	T_c	$2\Delta(0)/T_c$	$\Delta C/T_c$	$T_c/\omega_{\ln}$	μ^*
Sr	12.9 (12.7)	8.5 (8.4)	4.06	29.0 (28)	0.110	0.11
Ca	10.3 (17.4)	6.34 (6.6)	3.66	16.8 (11)	0.058	0.09
La	7.18 (6.7)	1.56 (1.5)	3.53	10.5 (2)	0.013	0.11

In conclusion, the first-principles calculations and Migdal-Eliashberg analysis presented in this work prove that the superconductivity in the APt_3Pt compounds is of conventional *ep* nature. These are the first three examples of superconductors that crystallize in an *antipolar* version of the crystal structure of the non-centrosymmetric heavy fermion $CePt_3Si$. The remarkable agreement with the experimental data allows us to make some conclusive statements. In contrast to $CePt_3Si$, where the Ce f states at the Fermi level have a large SOC, in APt_3P the SOC plays a marginal role, excluding the possibility of exotic pairing as proposed for SrPtAs [6]. We also did not find any signatures of a charge density wave instability as proposed in Ref 8. Instead, we found that superconductivity is conventional, with an *ep* coupling which is moderate in La, and much stronger in Ca and Sr, where Pt(1) breathing phonons couple to in-plane electronic states. $SrPt_3P$, where the breathing modes have low frequencies, belongs to the same class of low-frequency, strong-coupling superconductors, as the A15 and Chevrel compounds [13]. The low frequency phonon behaviour can be tuned by modifying the in-plane lattice parameter. Together with the possibility of controlling the polarity of the structure through suitable choice of the X atom, this makes APt_3X compounds a very promising new class of superconductors.

Acknowledgements: We would like to acknowledge A. P. Schnyder, O.V. Dolgov and R.K. Kremer for useful discussions.

Note: During the submission of this work, we became aware of a related study on lattice dynamics in APt_3P compounds [16].

[1] B.J. Kim et al., Phys. Rev. Lett. **101**, 076402 (2008); M.Z. Hasan and C.L. Kane, Rev. Mod. Phys. **82**, 30453067 (2010).
[2] Manfred Sigrist and Kazuo Ueda, Rev. Mod. Phys. **63**, 239 (1991).
[3] M. H. Fischer, F. Loder and M. Sigrist, Phys. Rev. B **84**, 184533 (2011).
[4] E. Bauer, G. Hilscher, H. Michor, Ch. Paul, E.W. Scheidt, A. Gribanov, Yu. Seropegin, H. Nol, M. Sigrist, and P. Rogl, Phys. Rev. Lett. **92**, 027003 (2004).
[5] Y. Nishikubo, K. Kudo, and M. Nohara, J. Phys. Soc. Jpn. **80**, 055002 (2011).
[6] Suk Joo Youn, *et al.*, Phys. Rev. B **85**, 220505; S. J. Youn, M. H. Fischer, S. H. Rhim, M. Sigrist, D. F. Agterberg, arXiv:1111.5058 (2011); J. Goryo, M. H. Fischer, M. Sigrist, arXiv:1208.2541.
[7] T. Takayama, K. Kuwano, D. Hirai, Y. Katsura, A. Yamamoto, H. Takagi, Phys. Rev. Lett. **108**, 237001.
[8] H. Chen, X.-F. Xu, C. Cao, and J. Dai, Phys. Rev. B **86**, 125116 (2012).
[9] I. A. Nekrasov, M. V. Sadovskii, JETP Letters **96**, 227 (2012).
[10] S. Baroni *et al.*, Rev. Mod. Phys. **73**, 515 (2001).
[11] We solved the Migdal-Eliashberg equations [*J. P. Carbotte, Rev. Mod. Phys.* **62**, *10271157 (1990)*] in the single-band case. The specific heat jump was obtained

from the second derivative of the free energy, according to [*O. V. Dolgov et al.,Phys. Rev. B* **72***, 024504 (2009)*].

[12] Our calculations employ density functional perturbation theory [10] within the generalized gradient approximation (GGA) as implemented in the Quantum-ESPRESSO package [*P. Giannozzi, et al., J. Phys.: Condens. Matter* **21***, 395502 (2009)*]. We use ultrasoft pseudopotentials and basis set cutoffs of 40 Ry and 400 Ry for wave function and charge density, respectively. We use an $8 \times 8 \times 8$ grid for zone integration in the self-consistent calculations, while a denser $16 \times 16 \times 16$ grid is used in the *ep* coupling calculations. The dynamical matrices are calculated on an $8 \times 8 \times 8$ grid, and phonon dispersions and DOS are then obtained by Fourier interpolation.

[13] F. Marsiglio and J.P. Carbotte, Phys. Rev. B **33**, 6141 (1986).

[14] The experimental space group is $P4/nmm$ (no. 129); the unit cell comprises two formula units ($f.u.$) and A, Pt(1), Pt(2) and P occupy $2a$, $4e$, $2c$ and $2c$ Wyckoff positions respectively. Structural relaxation (GGA) yields the following lattice parameters: Sr: a=5.898 Å, c=5.470 Å, z_{Pt2}=0.1362, z_P= 0.7227; Ca: a=5.758 Å, c=5.494 Å, z_{Pt2}=0.1357, z_P= 0.7303; La: a=5.838 Å, c=5.553 Å, z_{Pt2}=0.1418, z_P= 0.7719.

[15] We carefully checked the convergence of our phonon spectra, but we could not reproduce the dynamical instabilities reported by the authors of Ref. [8]. We believe that these are not physical, as we discuss later in the paper. The difference most likely stems from the different pseudopotentials employed in that work.

[16] Chang-Jong Kang, Kyo-Hoon Ahn, Kwan-Woo Lee, B. I. Min , arXiv:1207.6196.